THE ASTROPHYSICAL JOURNAL, 554:451–463, 2001 June 10

EVIDENCE FOR THE FLARE TRIGGER SITE AND THREE-DIMENSIONAL RECONNECTION IN MULTIWAVELENGTH OBSERVATIONS OF A SOLAR FLARE

L. FLETCHER,[1,2] T. R. METCALF,[2] D. ALEXANDER,[2] D. S. BROWN,[3] AND L. A. RYDER[4]

Received 2000 March 1; accepted 2001 February 12

ABSTRACT

Based on a multiwavelength data set and a topological model for the magnetic field, we argue that a M1.9 flare which occurred on 1993 May shows evidence of three-dimensional coronal reconnection in a spine-fan configuration. Images from the *Transition Region and Coronal Explorer* allow the detailed examination of the structures involved in the flare and preflare in the 171 Å (1 MK) EUV passband and the Lyα (10,000–20,000 K) passband. *Yohkoh* Hard X-ray Telescope maps the position of nonthermal electron precipitation and the Soft X-ray Telescope reveals preflare and flare heating on large and small scales. While the flare appears to be driven by changes in small-scale field close to the photosphere, near the interface between strong opposite magnetic polarities, the result is the disruption of large-scale field. We demonstrate how this observed activity on large and small scales, along with many other aspects of the flare, suggests a qualitative explanation in the three-dimensional reconfiguration of coronal magnetic field, following a small-scale flux cancellation at the photosphere.

Subject headings: Sun: corona — Sun: flares — Sun: magnetic fields — Sun: X-rays, gamma rays

1. INTRODUCTION

The phenomenon of the solar flare presents us with many and varied theoretical challenges. Not least of these is how to reconcile the expected small size of the flare trigger site with the (inferred) acceleration of great numbers of particles and the (observed) response of a vast coronal volume. It is generally believed that the flare trigger is a magnetic reconnection event, which facilitates reconfiguration of the magnetic field, as well as providing an environment in which particles can be accelerated. Theoretically, the thickness of current sheets in reconnection regions is comparable to the ion gyroradius, which is centimeters to meters in the corona, and observationally, all flare impulsive signatures, from hard X-rays (HXRs) to Hα imply impulsive phase heating and acceleration on the scale of hundreds to thousands of kilometers. Examples are spikes in the *Solar Maximum Mission* (*SMM*) Hard X-Ray Burst Spectrometer exhibiting structure down to hundreds of milliseconds (which suggests source sizes of <1000 km), the measurement by Canfield et al. (1991) of a particle precipitation area of $\sim 10^{17}$ cm^2, or observations with the *Transition Region and Coronal Explorer* (*TRACE*; Handy et al. 1999) which show impulsive extreme-ultraviolet (EUV) kernels not more than a couple of arcseconds in each dimension. However, the much larger scale effects of flares are well known. With the *Yohkoh* Soft X-Ray Telescope (SXT; Tsuneta et al. 1991) we see heating over volumes of $\sim 10^{30}$ cm^{-3} throughout the flare, ejection of huge quantities of plasma, and the filling of loop systems on the order of 10^{10} cm long. The connection between the localized trigger and its global effects is still largely unexplored.

To understanding this connection it would appear sensible to start by identifying the trigger site (by which we mean the location of the reconnection event) and its significance in the larger scale magnetic topology of the system. However, because of its small size, the arguments used in identifying this site are necessarily indirect. Tsuneta et al. (1992) have argued that cusped loops seen with SXT in long-duration events (LDEs) indicate coronal reconnection. This argument is based on two observations: (1) the similarity between the shape of the field implied by these cusps, and the shape of field lines entering a two-dimensional "*x*-" or "*y*-"type reconnection region, and (2) the evolution of the soft X-ray (SXR) loops in a manner consistent with that expected from a high, upward-moving reconnection site. McKenzie & Hudson (1999) observed infalling dark blobs above the top of a postflare LDE arcade (15,000 km above the photosphere) which they argue are the cross sections of loops in the process of relaxing, following reconnection in the corona above the arcade. Other evidence of a coronal reconnection site comes from Aschwanden et al. (1996a, 1996b), who use BATSE high-precision hard X-ray (HXR) time profiles to determine the time lags between electrons of different energies, and infer an acceleration site in the high corona (an average distance of 44,000 $\pm$ 6000 km above the photosphere). For other events, apparent changes in the three-dimensional topology of a pair of interacting magnetic loops before and after a flare (e.g., Hanaoka 1997; Nishio et al. 1997) suggest coronal reconnection where they intersect.

With new, high-resolution flare observations, and developments in the modeling for three-dimensional magnetic fields, our understanding of the flare trigger and its impact on the large-scale coronal field is being expanded. Although still in its infancy, the comparison of extrapolated coronal fields with high-resolution flare images (made possible on a regular basis by the ready availability of excellent quality space-based images and magnetograms) is proving to be a rich field, and there are many indications of a relationship between the predicted location of magnetic separatrix structures, or separators, and the site of flaring activity. For example, Demoulin et al. (1993) showed that Hα flare kernels tend to occur at the locations of predicted separators with the chromosphere. Longcope & Silva (1998) com-

[1] Department of Physics and Astronomy, University of Glasgow, Glasgow G12 8QQ.
[2] Lockheed-Martin ATC, Solar and Astrophysics Laboratory, Department L9-41, Building 252, 3251 Hanover St., Palo Alto, CA 94304.
[3] Department of Mathematical and Computational Sciences, University of St. Andrews, St. Andrews, Fife KY16 9SS, UK.
[4] On leave from University of California, Davis.

pared the magnetic field topology of a flare on 1992 January 7 with sites of heating (observed with *Yohkoh* SXT) and particle precipitation (observed with *Yohkoh* Hard X-ray Telescope [HXT] and in microwaves), finding that these correspond well with the predicted sites of magnetic separators and their footpoints, respectively. Recently, Aulanier et al. (2000) studied the 1998 July 14 flare, observed in detail with *TRACE*, and find a "spine" and "fan" field configuration (as we suspect to be the case for the present case, described in § 4), and show that the flare ribbons and changes in the large-scale corona may be associated with evolution in this complex field.

In this paper, we continue in the same vein, examining an impulsive M1.9 flare which was well observed by several instruments. Our novel development is the creation of a topological model for the evolution of the magnetic field under the action of photospheric driving, which we compare with observations. In doing so, we call upon recent topological modeling of the evolution of three-dimensional magnetic fields in response to photospheric footpoint driving (Priest et al. 1997; Brown & Priest 1999), and use data from *TRACE*, *Yohkoh* HXT (Kosugi et al. 1991) and SXT, and the *SOHO* Michelson Doppler Imager (MDI). This paper is intended to present the flare observations and make an initial comparison with the topological model.

On the basis of this model, we identify the driver and the site of the flare trigger, and explain qualitatively many aspects of the flare evolution, particularly the link between large- and small-scale activity. Our observations are consistent with a scenario in which photospheric flux cancellation leads ultimately to a rapid topological reorganization of the large-scale coronal magnetic field, by reconnection at coronal separators or a coronal null. This produces coronal heating and material ejection, and multiple sites of small-scale activity in the lower atmosphere.

In § 2 we list the data used in the study, and the analysis thereof. Section 3 describes the flare event, and in § 4 we present the model for the magnetic field and interpret the event in the context of this model. Further discussion is presented in § 5.

2. DATA SUMMARY

On 1999 May 3, AR 8524 was a decaying active region located at 22° north, 62° west. The flare which we consider attained *GOES* M1.9 level, and lasted from 23:07 to 23:13 UT, with a peak at 23:11 UT. The region also showed a small *GOES* flare (B5.9), starting at 22:38 UT, peaking at 22:41 UT, and with a total duration of 5 minutes. Figure 1 shows the *GOES* curve for the interval around the flare, indicating the times of SXT, *TRACE*, and HXT coverage.

The *TRACE* data set consists of full-resolution 171 Å and Lyα images with pixel size 0.″5 × 0.″5. The cadence of the observations was approximately 1 minute in each wavelength, with some interruption to the 171 Å cadence (see Fig. 1) when a series of Lyα images was made. The principal lines in the 171 channel are Fe IX/Fe X, 0.5–1.5 MK with a peak at 0.95 MK, while the Lyα channel images plasma between 10,000 and 30,000 K. The data are prepared by removing cosmic-ray hits, subtracting the detector pedestal, and normalizing to 1 s exposures.

The SXT preflare data are mostly in the AlMg filter, with full-resolution images (pixel size 2.″46 × 2.″46) at a cadence of approximately 16 s. The flare mode data are full-resolution exposures at a cadence of 2–4 s cycling through

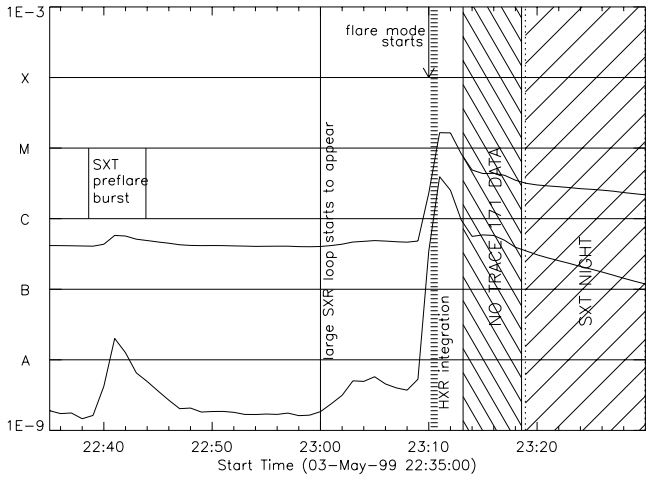

FIG. 1.—*GOES* curve for the preflare and flare phases, with indications given of data coverage and significant times in the flare.

the Al.1, AlMg, Be, and Al12 filters. These four filters together span a temperature range of 2–50 MK, with temperatures greater than 10 MK often observed in flares (e.g., Tsuneta 1996). The SXT data preparation (see Alexander 1999) involves dark current and leak subtraction, normalization, and coregistration. The data are then passed through a descattering routine which deconvolves with the known scattering properties of the SXT optics (courtesy of D. McKenzie) and corrected for vignetting.

The HXT images in all four channels were made over an interval of 50 s between 23:10:00 UT and 23:10:50 UT. These images are reconstructed with the "Pixon" method (Metcalf et al. 1996). The pixel size of the reconstructed images is 2.″5 × 2.″5. The flare occurred while HXT was in calibration mode, which means that pulse heights from the instrument are binned into 64 rather than the usual four energy bins, and the data accumulation time is 8 s rather than the usual 0.5 s. Thus, the time resolution of these observations is, unfortunately, significantly poorer than HXT usually attains. MDI synoptic magnetograms were also used for magnetic context. The pixel size is 2.″0 × 2.″0 and the cadence 96 minutes.

Much of our analysis involves the coalignment of images from different instruments, which is a difficult business. Pointing information is often not good enough to obtain the precise co-alignment needed for detailed study. For example, it is known that thermal bending of the *TRACE* guide telescope, which varies around the orbit and through the year, leads to a variation in the pointing of at least a few arcseconds (T. D. Tarbell 1999, private communication; De Pontieu 1999, private communication). We have used the pointing information as a first step and thereafter used feature co-alignment on large and small scales, occasionally comparing images at different times. However, we must be wary of feature co-alignment on images made in two different passbands, and our conclusions will keep this in mind.

3. FLARE OBSERVATIONS

3.1. *The Magnetic Field*

MDI magnetograms from the 36 hr preceding the flare show the emergence of a small bipole into the trailing negative polarity of the AR. The negative polarity of this bipole is slowly dispersed, leaving a positive field concentration

(PFC), more or less surrounded by the negative field of the sunspot. Figure 2 shows the preflare MDI magnetogram made closest in time to the flare, at 1999 May 3 22:24 UT (35 minutes before the flare). The line-of-sight field strength in the PFC was 250 G. Comparison of the 1999 May 3 00:00 UT magnetogram differentially rotated to 22:24 UT and the actual magnetogram made at 22:24 UT shows that the "proper motion" of the PFC is southward into strong negative field.

3.2. *The Preflare Phase*

TRACE 171 Å and Lyα images from about 22:30 UT onward (i.e., 30–40 minutes before the flare) show two small, looplike brightenings, each 5″–10″ long. These are located near the southwest boundary of the PFC and the surrounding negative field (see Fig. 2) and persist throughout the entire preflare phase. There may also be evidence of a small, dark, curved filament in the 171 Å images (Fig. 2), approximately following the outline of the PFC. SXT AlMg filter images around 22:30–22:40 UT show a bright core of emission, in the form of a loop (Fig. 3, *upper left panel*).

The B5.9 preflare burst is seen clearly in the SXT AlMg images, between 22:38:36 and 22:43:53 UT. It occurs in or near the SXT core. The small *TRACE* preflare loops brighten in 171 Å between 22:43 and 22:46 UT. This burst appears to involve only very local field, on a scale of 10″ or so, concentrated around the edge of the PFC. There is no evidence that large-scale field is involved during this precursor event.

At 23:00 UT the intensity in the SXT core increases again, leading quickly to pixel saturation and bleeding. At this time we also have the first clear signs of the participation of the larger scale field. A large loop starting near the SXR core begins to brighten at 23:00 UT and at 23:03 UT is quite clear (Fig. 3, *upper right panel*). It extends to a region of positive field visible in MDI (though there could be unresolved mixed polarity). The SXT loop and core intensity increases steadily in the build-up to the flare (Fig. 3; *lower left panel*); no sign of this brightening is visible in *TRACE* preflare data. This suggests that the preflare heating results in an increase of only the high-temperature emission measure.

3.3. *The Impulsive Phase in Hard X-Rays and EUV*

Yohkoh flare mode starts at 23:10:00 UT. The impulsive phase HXR emission peaks at 23:10:20 UT and appears as a single compact source. EUV at 23:10:05 shows a set of bright kernels. The development of the flare in *TRACE* 171 Å is shown in Figure 4. The diffraction patterns generated by the mesh which supports the *TRACE* front filters is clearly visible, and marks the position of the strongest sources. The intensity profiles of the three strongest EUV sources, at positions (813″, 370″) (position of the southernmost *TRACE* preflare loop) (797″, 390″), and (802″, 387″) along with the HXT profile, are shown in Figure 5. The peak in EUV emission occurs within 90 s of the HXR peak. The impulsive appearance of the EUV kernels may suggest that they are, like the HXRs, in some way connected with beam excitation of the chromosphere (see § 4 for more discussion). Synchronized impulsive UV (or EUV) and HXR flare maxima have been observed on previous occasions (e.g., Woodgate et al. 1983; Donnelly & Kane 1978).

During the time for which we have HXT images, the SXT images are saturated and it is not possible to co-align with *TRACE*. Therefore, we co-align *TRACE*, SXT, and HXT using the *TRACE* image at 23:12:37 UT, where a bright loop is visible at (810″, 370″), and an SXT image at 23:12:46. By this time the SXT automatic exposure control has reduced the exposure times sufficiently that we can see the flare core in the Be filter. We assume that this core is the same feature as the *TRACE* bright loop (it has a similar size, orientation, and location) and align on this. The SXT and reconstructed HXT images are aligned to better than 1″. The result of this co-alignment is shown in the left and center panels of Figure 6. We estimate that the relative position of the *TRACE* and HXT sources found in this way is at least as good as 5″ in x- and y-directions combined (the largest error coming from the *TRACE*/SXT co-alignment). It is $\sim +2''$ north-south and $-2''$ east-west displaced from a

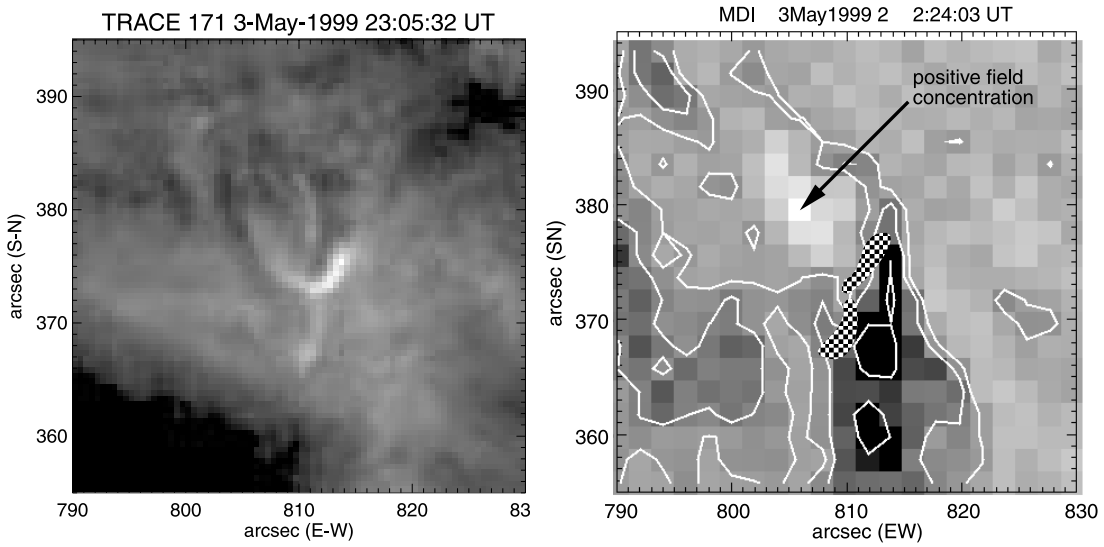

FIG. 2.—*TRACE* 1.71 Å preflare image, and *SOHO*/MDI preflare magnetogram. Contours (of negative field only) are at (−700, −200, and −10 G). Positive field is shown in white and negative field in black. Persistent preflare brightenings in *TRACE* are located near the interface between positive and negative field elements, shown by the hatched areas.

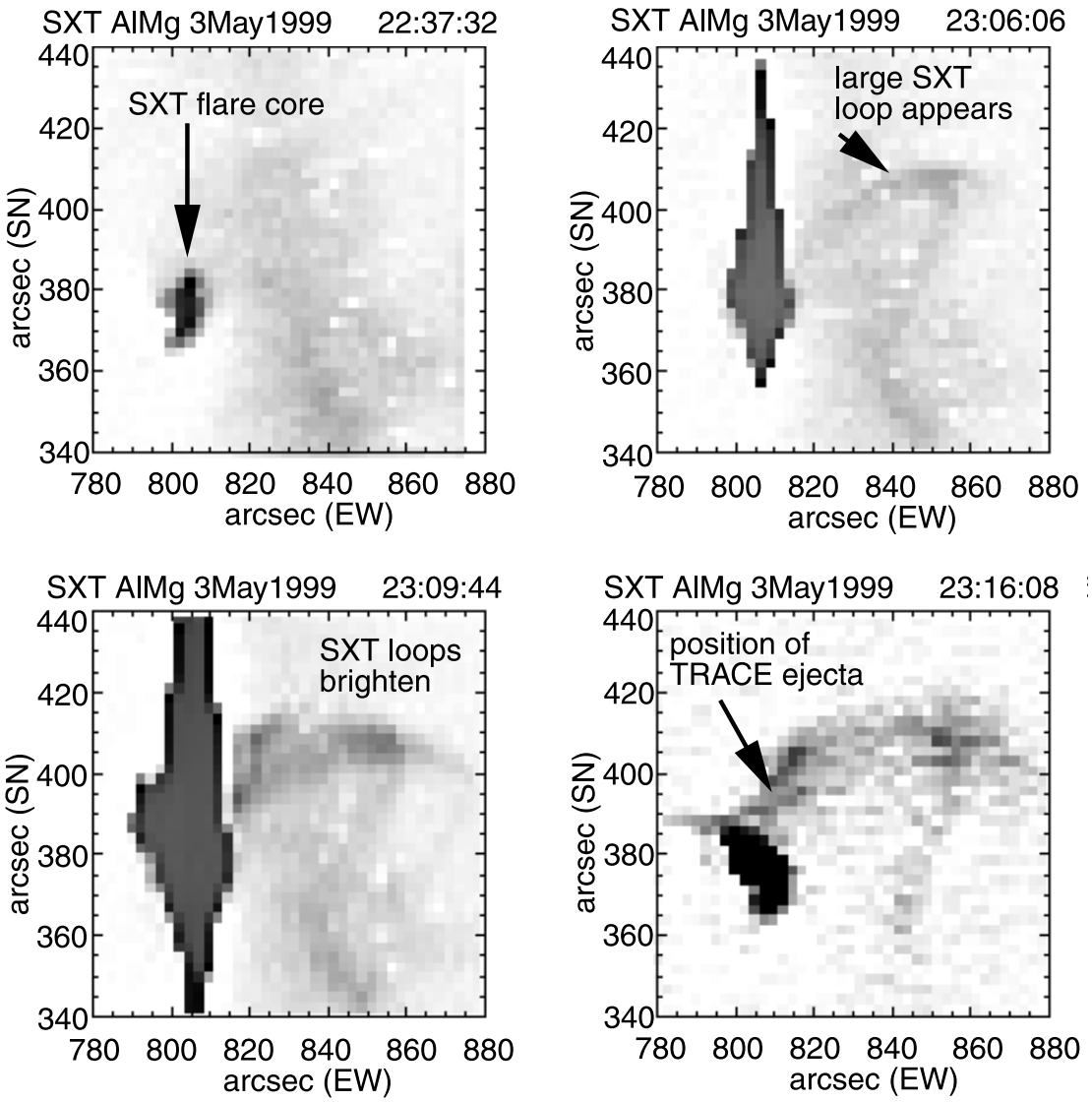

FIG. 3.—SXT AlMg images of the region before and after the B5.9 event (*top panels*), near flare maximum (*lower left panel*), and in the postflare phase (*lower right panel*). Before the B5.9 flare only a compact hot core is visible, apparently with the form of a small loop. After the B5.9 flare, and in the lead-up to the M flare, a large loop originating near the saturated core starts to brighten. During and after the flare, more loops become visible.

co-alignment made "blind" from the instrument pointing information. Figure 7 shows the HXT sources at 23:10:21 UT in each of the four energy channels, overlaid with contours of a *TRACE* image at 23:11:42 UT. The location of the HXT source, particularly at high energies, correlates well with the small, bright, *TRACE* EUV loop.

TRACE 171 Å also offers evidence of the excitation by the flare of more distant locations. In the exposures at 23:11:42 UT and 23:12:37 UT a tiny brightening is visible at (845″, 360″), or about 90,000 km from the main flare site (assuming that the brightening occurs low in the atmosphere). The brightening is also very strong in Lyα, and corresponds to the end of the large SXT loop.

3.4. *Material Ejection*

At 23:11:42 UT the first ejecta are visible in *TRACE* 171 Å and Lyα, in the north of the group of flare kernels. By measuring the position of the leading edge of the ejecta, we determine a projected (minimum) speed of $\sim$170 km s^{-1}. The ejecta appear to originate around the edge of the oval defined by the EUV flare kernels. The ejecta appear vertically structured, with the overall shape being that of a cusp (Fig. 4). This suggests channeling by magnetic field. The direction of the ejecta corresponds to that of the large SXR loop (see Fig. 6, *center panel*), which brightens significantly between about 23:11 and 23:13 UT. The observed material ejection may be partly responsible for the SXT brightening, through an increase in the emission measure.

A temperature map (Fig. 6, *right panel*) made from images summed between 23:13:34 and 23:17:50 UT (i.e., 3–7 minutes after the impulsive phase) shows that the bright core of the flare and the lower part of the large loop is at $7 \pm 2 \times 10^6$ K. Toward the top of the large loop the temperature is $1.5 \pm 0.5 \times 10^7$ K. These are of course time- and line-of-sight integrated values, but do give an indication at least of relative temperatures. [Note that instrumental scattering leads to errors in the temperature determination, and although we have corrected for this as best we can, in practice values of log (T_e) > 7.2 should be treated with caution (D. McKenzie, private communication)].

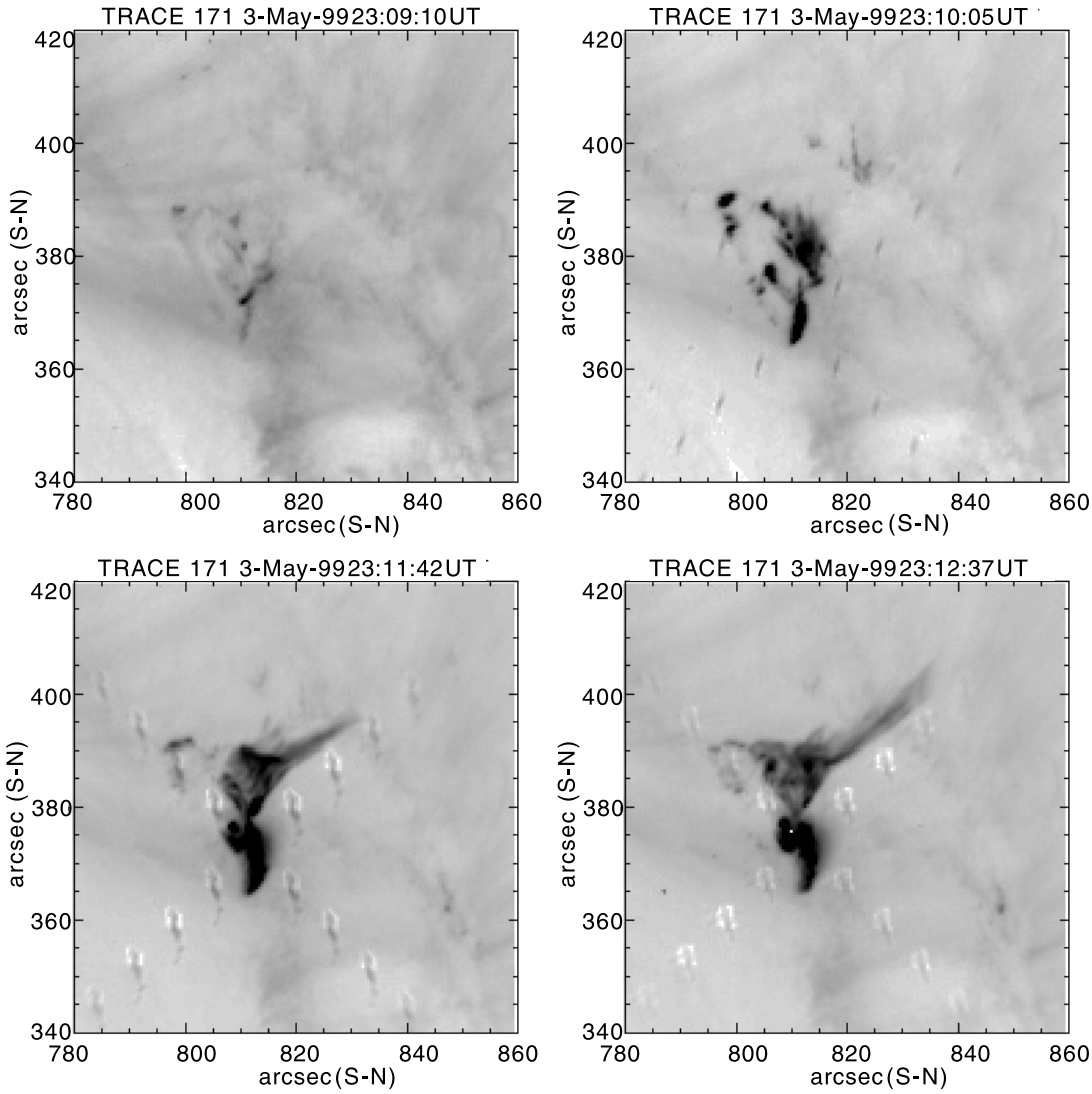

FIG. 4.—*TRACE* 171 Å images of the flare site made around the impulsive phase. The images have been approximately corrected to remove the worst of the instrumental diffraction pattern. Near the time of the HXR impulsive phase (23:10:00–23:10:50 UT) the *TRACE* emission is confined to a few bright kernels; shortly thereafter, the kernels disappear, a small loop brightens, and material ejection starts. Note the complicated shape of the ejected material.

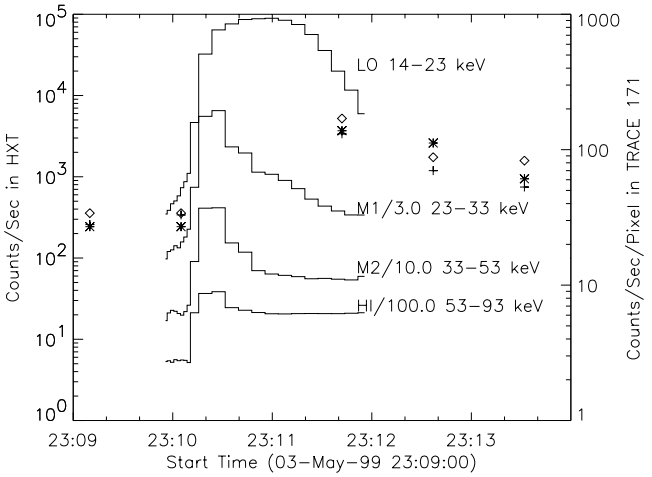

FIG. 5.—Time profiles of *TRACE* EUV emission at three kernels (*diamonds*: [797″, 390″], *stars*: [802″, 375″], and *crosses*: [813″, 362″]) and the HXT four-channel emission. The HXT emission starts to rise when the EUV emission is still at its preflare level, but the peak of the EUV emission is no more than 90 s after the HXR burst.

The ejection continues for at least 11 minutes, and the position where the ejection originates moves round the structure. In Lyα, a small bright blob can be seen moving anticlockwise around the footpoint oval, apparently at the base of the ejection. A set of difference images shows this well (Fig. 8). The small circles and dashed lines mark the position of the moving brightening. Taking into consideration projection effects, we calculate an average speed for this brightening of 44 ± 25 km s^{-1}. The traveling blob may indicate some propagating magnetic signal or disturbance traveling through the field, such as might occur during the "unzipping" of a filament, or systematic field reconfiguration or destabilization. We return to this matter in § 5.

4. INTERPRETATION OF THE EVENT

The observations described above clearly show both small- and large-scale activity in this flare. The preflare emission in *TRACE* EUV wavelengths is concentrated near the interface between strong oppositely signed fields in two small and distinct sources. Yet between the preflare and the

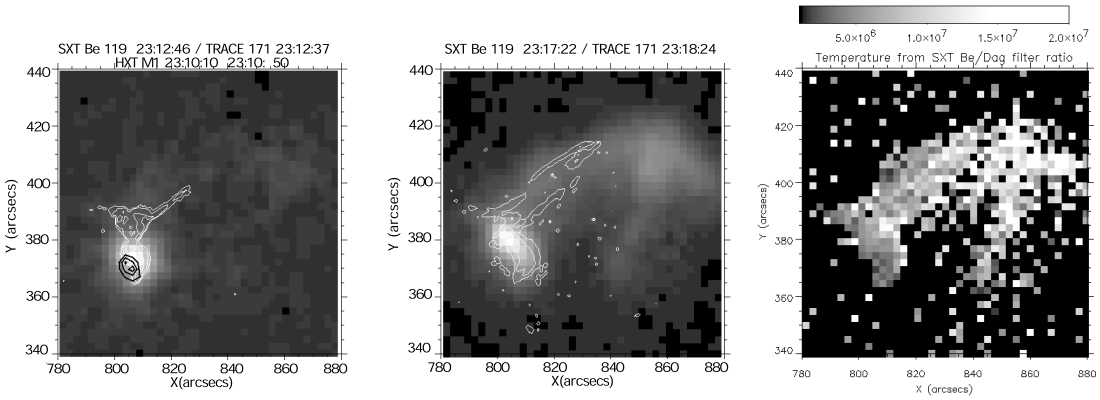

FIG. 6.—Overlay of *TRACE* (*white contour*), SXT Be filter (*gray scale*), and HXT M1 channel (*black contour*) emission shows the relationship between the HXR footpoint source, the *TRACE* ejecta, and the large SXT loop, close to the impulsive phase and during the postflare phase. The right-hand panel shows the temperature derived from the Be/AlMg filter ratio (data summed between 23:13:34 and 23:17:50 UT)

flare phases, a much larger loop ending near these sources becomes apparent in SXT. Throughout the event, while the most intense SXT flare emission comes from a small core, 10″–20″ long, the large SXR loop continues to increase in intensity. Similarly, while the EUV emission is strongest first in a number of flare kernels, then in a single bright loop (presumed to be the same as the SXT core) there are also large-scale up-flows of million-Kelvin material starting from a location several thousand kilometers to the northeast of the bright loop. HXT maps show a single source, located near the bright EUV loop (forward modeling, see § 5, indicates that a large volume of coronal plasma is necessary to supply the electrons that produce the HXR source).

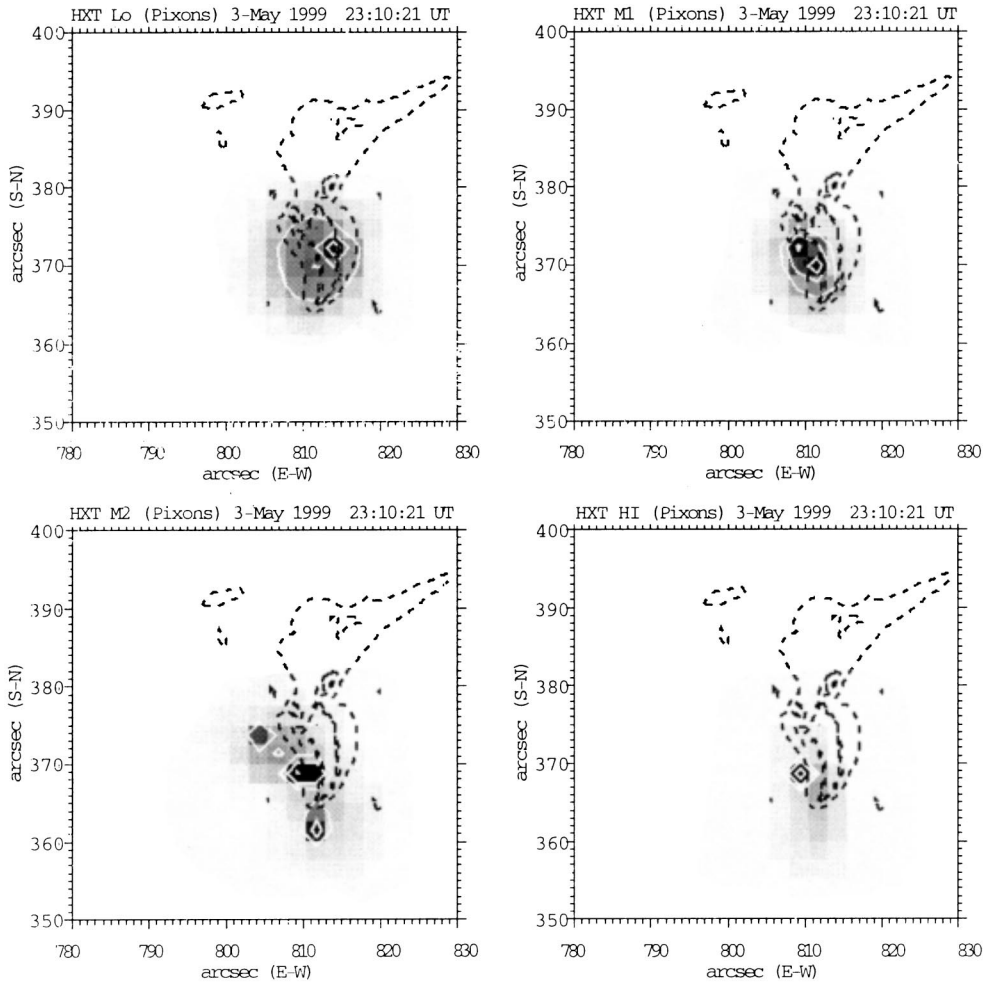

FIG. 7.—Reconstructions of the HXT emission in each of the four energy channels, made using the "Pixon" method. The contours are at 12.5%, 37.5%, and 75% of the maximum intensity in each image.

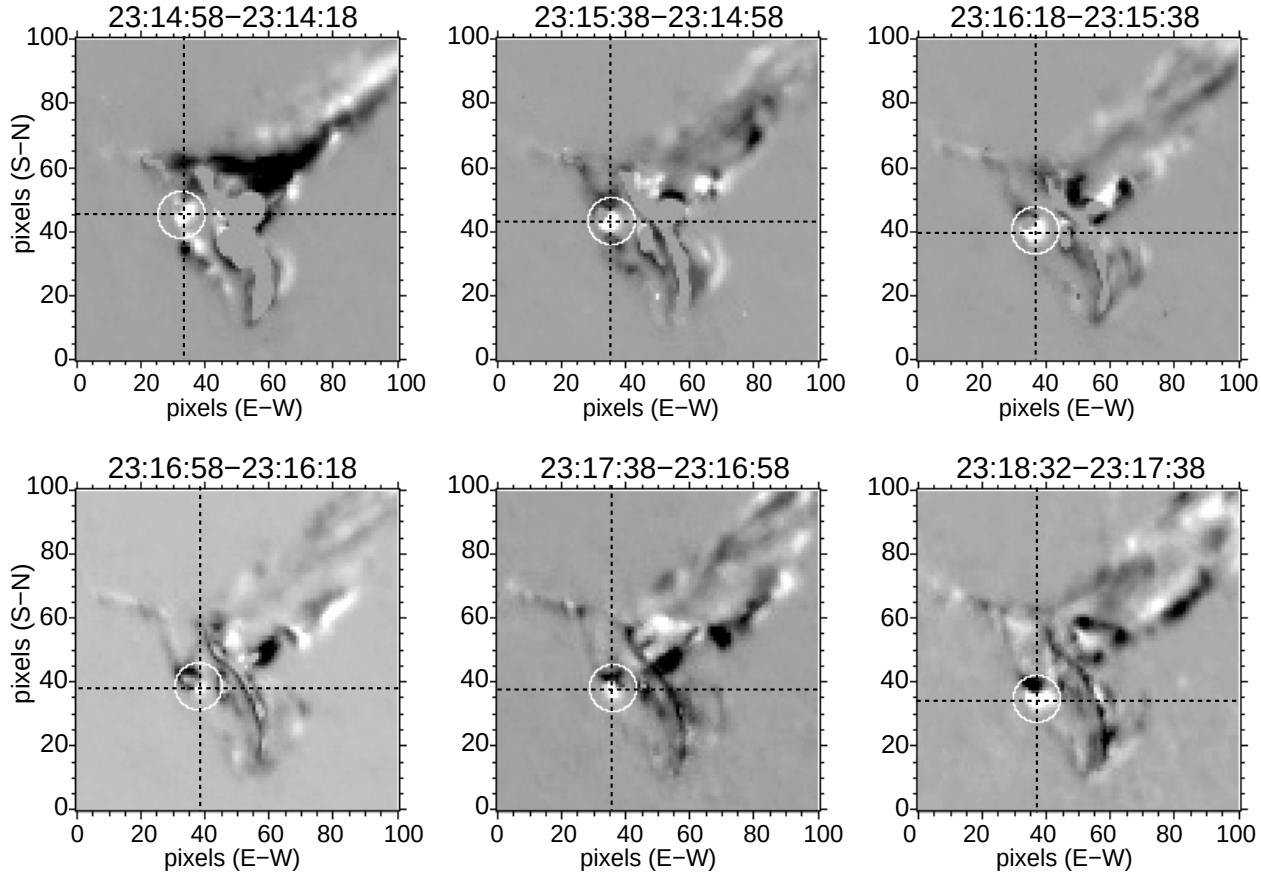

FIG. 8.—Sequence of Lyα difference images, of the flare ejection phase. White corresponds to an enhancement in emission between the exposures, and black to a decrease. Portions which are saturated stay the same, and are gray but with a well-defined edge. The moving dark/white or gray/white feature, outlined with a circle, corresponds to a blob of emission which moves around the base of the erupting structure. The position of the centroid of the brightening in each image is indicated with dashed lines.

4.1. *The Local Magnetic Field*

In attempting to assimilate the observations into a single consistent model, we look first at the magnetic field in this region. The preflare MDI magnetogram shows an isolated positive polarity (left behind from the emerged bipole) apparently surrounded by negative AR field. This suggests a peculiar coronal magnetic field consisting of a small flux system nested inside the overlying active region field. To confirm this, we have performed a field extrapolation from the MDI magnetogram. Because of the location of the AR, close to the solar limb, the line-of-sight field measured by MDI is close to horizontal. So to better understand the polarities of the magnetic field involved in the flare, and to map reliable neutral lines, we first performed a potential field extrapolation of the MDI data using the line-of-sight field as the boundary condition. We then treated the computed potential field at the photosphere as a vector magnetogram and deprojected the field to simulate an observation at disk center. The resulting "magnetogram" uses the vertical magnetic field, rather than the line-of-sight magnetic field, to map field polarities and neutral lines. This "magnetogram" and selected reconstructed field lines are shown in Figure 9.

Although a potential field is assumed, we consider the resulting "magnetogram" to be considerably more reliable than the line-of-sight magnetogram. We could equally well have used a linear (or even nonlinear) force-free field extrapolation rather than the potential field extrapolation; however, we have no objective method for determining the value of α in the absence of vector field measurements from MDI.

In Figure 9 we see that the PFC is indeed surrounded almost entirely by negative field. The PFC is connected to surrounding negative field by short magnetic connections forming an arcade. The PFC and the arcade linking it to surrounding negative polarity form a small closed flux system, within the larger scale flux system of the active region. Any two-dimensional cut through this system will give a magnetic field configuration looking like the X-type field proposed for "anemone" jets by Shibata et al. (1992, Fig. 5*c*, *middle panel*) and strongly suggests that in three dimensions the topology will include a coronal null somewhere above the PFC. In this case, the interface between the two flux systems would be a dome of separator field lines, joining the coronal null to the surface. The flare itself, seen in SXT, bears considerable resemblence to an SXT jet, with a bright core at the "footpoint" of an outflow of a few hundred km s^{-1}. However, the SXT "ejecta" are not well collimated, as is found in SXT jets, but are clearly looplike, and the detail revealed by *TRACE* of the core and the jet indicates clearly that this flare is not a two-dimensional phenomenon. Although Shibata and coworkers have modeled the jetting process in extensive two-dimensional MHD simulations, we believe that we should start to think

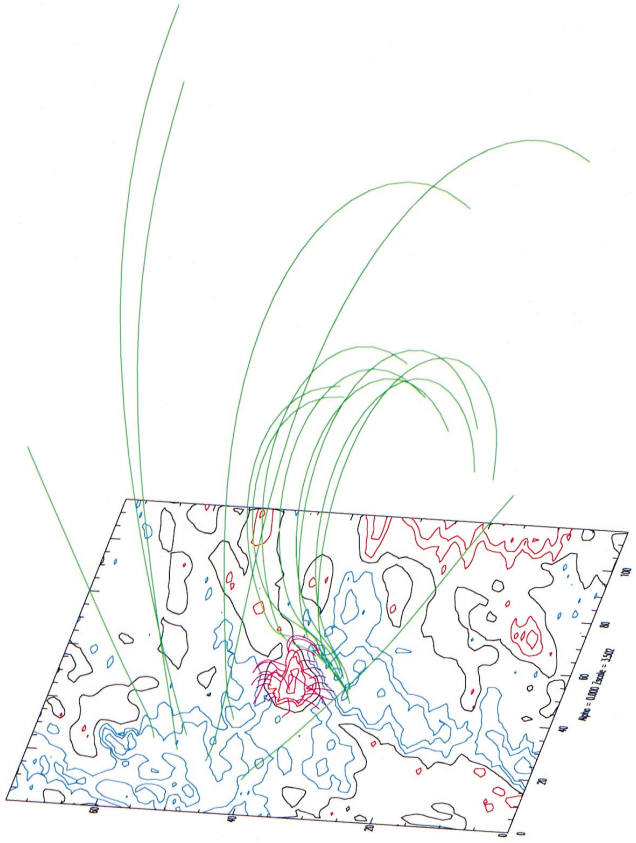

FIG. 9.—Potential field lines, reconstructed using the MDI magnetogram of 1999 May 3, 22:24:03 as the photospheric boundary. Units are MDI pixels (2.″0) east-west along the long edge, and south-north along the short edge. The magnetic field has been deprojected to simulate an observation at disk center, which has led to distortions since the active region is very near the limb. Contours of the vertical component of the positive and negative fields are shown in red and blue, respectively. Short field lines linking the included positive polarity with the surrounding negative polarity are in purple, and longer field lines are shown in green.

beyond two-dimensional models for this event and investigate simple three-dimensional interpretations.

The topology that we find is in fact identical to the "embedded bipole" topology described by Antiochos (1998). In such a topology, one would expect a coronal null to exist, and a discrete-source representation (see § 4.2) indicates that one is indeed present, although we have not been able to locate it in the extrapolation from the magnetogram. We expect that this is due to the coronal null (theoretically) being located rather close to the photosphere, because of the very unbalanced magnetic charges present; so close that its height above the photosphere approaches the grid resolution in the potential calculation (set by the pixel size), making it very difficult to find.

Sweet (1969) pointed out that the existence of independent three-dimensional flux systems separated by intersecting magnetic surfaces is necessary for the formation of current sheets (at which reconnection takes place) and proposed that such a geometry might exist in flaring regions. This basic concept has been significantly developed by, e.g., Lau & Finn (1990), Priest & Titov (1996), and the various magnetic structures classified. In three dimensions, reconnection takes place at a fan (a set of field lines directed away from a null, such as the separatrix dome), a spine (a singular field line approaching a null), or a separator (the intersection of two separatrix surfaces). If, as we suspect, a separatrix dome or coronal null exists in our field, then reconnection at such structures would provide a link between the small-scale field within the separatrix dome and the large-scale field of the active region.

As mentioned above, there are indications that separators or separatrix structures are significant locations in flares, and Longcope (1996) and Longcope & Silva (1998) have developed an elegant model for the storage and release of magnetic energy at separator field lines, which we describe briefly here. If reconnection cannot take place immediately in response to stressing of the coronal field by footpoint motion (and the existence of flarelike phenomena is an indication that energy can indeed be stored in the corona for some time) then coronal current must build up. Longcope (1996) proposed that the minimum energy state for a current-loaded corona is that in which all the current is concentrated in (untwisted) ribbons in the close neighborhood of magnetic separators. This is known as the minimum-current corona (MCC) model. One prediction of this model is that the separator locations will also be locations of Joule heating; a further suggestion is that they will be preferential locations for reconnection leading to a flare. It is reasonable to expect that the coronal current cannot build up indefinitely as footpoint stressing continues. Longcope proposed that this coronal stress can be relieved once the separator current is driven beyond a certain threshold at which reconnection can occur. This process was described by Longcope in an ad hoc manner as "stick-slip" reconnection. The threshold condition might correspond, for example, to a level or scale of turbulence in the the current sheet generating suitable conditions for a tearing mode. In any case, according to the MCC model, coronal separators are important in defining the location of both heating and reconnection in preflare and flare events. We return frequently to this concept in our further discussions.

4.2. *A Topological Field Model*

We noted earlier that the PFC is drifting southward into a region of strong negative field. As a working hypothesis, let us suppose that as this happens flux cancelation occurs at the photosphere. This leads to the small-scale heating seen before the flare and preflare, and as the photospheric flux is moved around, and magnetic charge canceled, energy is input into the coronal field. The field is thus stressed. Let us further suppose that the relaxation of this stress occurs via magnetic reconnection, resulting in topological changes in the coronal field. By studying the topological changes resulting from this series of events we hope to understand the flare behavior.

We model the topological evolution by generating a series of (static) coronal potential fields corresponding to successive arrangements of a discrete source representation of the photospheric magnetic charge distribution. Each arrangement will lead to a somewhat different coronal topology from the previous one. To interpret this sequence of static fields as a sequence in time we must postulate that magnetic reconnection will take the field from one arrangement to the next. It should be pointed out here that to understand the topological changes we need say nothing about the point in time or the rate at which the reconnection happens, whether it happens smoothly and continuously along with the driving, or in small, intermittent

bursts, or in one catastrophic release. With the two conditions that reconnection is permitted in some form and that the real field topology can be well represented by our potential field extrapolation, the sequence of static field solutions will show the changes in coronal field connectivity which must (eventually) take place in response to the photospheric changes.

It is now generally accepted that reconnection occurs during solar flares, so perhaps our first condition needs little justification. There can be litte doubt that reconnection occurs in the solar corona: for example, in high-resolution *TRACE* observations of the interaction of newly emerged and preexisting flux systems (e.g., Schrijver et al. 1999), field linkages appear rapidly and "spontanteously." Here, reconnection is apparently proceeding with relative ease, in the absence of anything which we would recognise as a flare. The problem with flares is that the classical resistivity is very small, and resistive reconnection proceeds slowly—far too slowly to explain flare energy release rates. Even models of fast resistive reconnection with nonclassical rates, e.g., Craig & McClymont (1999), have trouble matching flare requirements. But reconnection is an ill-understood process, and despite theoretical difficulties we work on the assumption that it does occur in flares.

Our use of potential (zero free energy) field extrapolations does require justification. Although it has been used in the past to describe the preflare corona (e.g., Aulanier et al. 2000), a potential field extrapolation is clearly not the best representation for a field which we presume is being stressed by footpoint motions. A preflare field must be in a nonpotential state, otherwise there would be no free energy for the flare. Therefore, some "energy-bearing" model would do a better job at describing field line shapes and orientations. However, we justify the use of a potential field by reiterating that we are interested at this stage only in the topology, i.e., the connectivities, of the magnetic field lines, and how these change, rather than their exact orientations and shapes. It has recently been demonstrated (Brown & Priest 2000) that in general the topology of a potential field is expected to correspond well to the topology of a linear (or weakly nonlinear) force-free field extrapolated from the same set of source charges, out to some distance determined by how nonpotential the field is. There do exist particular symmetric configurations of photospheric charge in which this equivalence does not hold (e.g., Hudson & Wheatland 1999), but the relatively small topological changes which we see when we perturb our system indicate that we are not working with such a configuration.

4.3. *Perturbation of the Topological Field Model*

We represent the photospheric field by one strong positive and several weaker negative sources. The sum of negative and positive flux is less than zero, the balancing positive flux being outside the calculation box and assumed not to affect the topology within. The static potential field generated by these sources is calculated, and a representative starting configuration is shown in the top left panel of Figure 10.

The topological extrapolation shows a number of features that will be important in the further interpretation of

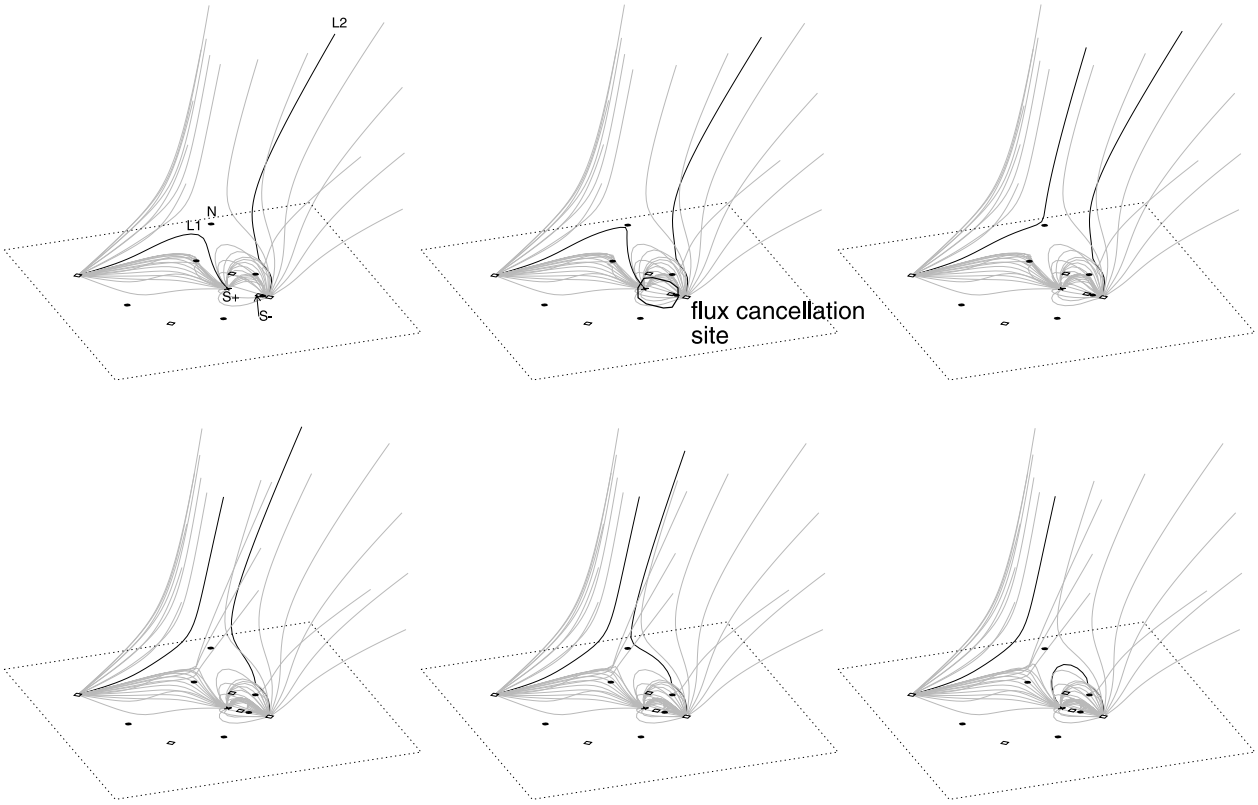

FIG. 10.—Series of potential field reconstructions showing some key configurations of field in the process of reconnecting though the null from inside to outside the separatrix dome, and vice versa. Note that the null does not lie in the plane of the footpoints, but is a coronal null. The images are made at unevenly spaced time intervals ($t = 0$, 5, 6, 18, 19, and 20, in arbitrary units), showing that the reconnection event proceeds rapidly compared to the slow driving of the field toward the null.

the event. First of all, we find the presence of a coronal null, as suggested by the field extrapolation from the magnetogram. While magnetic nulls are not uncommon in discrete source representations, these are usually in the photosphere, and a coronal null such as we find requires rather particular source arrangements (Brown & Priest 2000), one of these being a single source of one sign surrounded by sources of the other sign—such as we have. In our topological extrapolation, the existence of a coronal null is found to be rather robust to changes in the number, size, and distribution of the negative sources around the single positive source, so long as the sum of the negative and positive charges is less than zero. So while the discrete source distribution is an approximation to the observed field distribution rather than an exact representation, we consider that the null we find to be strong evidence for a coronal null in the real field. A coronal null in three dimensions is associated with spine and fan field lines, as described earlier.

To our starting configuration, we simulate the application of slow (compared to the Alfvén speed) photospheric driving which causes the positive field and negative field to the south to approach one another and cancel (in reality they might submerge or annihilate). This is done in a series of steady-state calculations in which a string of charges "break off" from the negative source and move toward the positive source. When each negative charge touches the positive source, we remove the negative charge and an equal amount of positive field. For each new configuration of photospheric charges, a static, three-dimensional potential field is calculated, and the series of fields emulates series of topological changes which the coronal field will undergo in response to photospheric driving.

Several frames from the series of calculations are shown in Figure 10, and two particular field lines (picked out in black) are chosen to illustrate the changes which occur in connectivity. Flux cancelation is taking place between positive source S+ and negative fragment S−, which is moving toward S+. In the top half of the panel we see a closed field line (L1) rise to approach the coronal null (N) and "reconnect" through to large-scale AR field (to the edges of the calculation box). In doing so it has passed from inside to outside the separatrix dome via the fan. Meanwhile, a field line L2 from outside the separatrix dome approaches the null from above, and "reconnects" via the spine to S+. The whole process thus brings field lines from outside the separatrix dome to inside, and vice versa. Of course, not all field lines are shown, and in practice for each field line that opens, another closes "simultaneously" to keep $\nabla \cdot \boldsymbol{B} = 0$. This illustrates how locally canceling field affects the global configuration.

Figure 11 shows in two dimensions how this occurs. As small-scale flux disappears from inside the separatrix dome, the dome distorts and field outside moves inward. This results in the external field becoming stressed as it adopts a nonpotential configuration, and relaxation must occur via reconnection at the null, as fan or spine reconnection. Not illustrated in this two-dimensional picture is the fact that within the separatrix dome each negative source forms, together with part of the positive, a separate flux system partitioned from its neighbors by separatrix surfaces. The internal field is also distorted by the flux cancellation, and a similar process of reconnection through separatrix surfaces will also occur between the segments within the separatrix dome.

Note that the inward relaxation of reconnected field lines through the separatrix dome may be a particular theoretical example of the general conjecture (Hudson 2000) that a shrinkage in the magnetic field accompanies the flare energy release. The observations presented here do not show the shrinkage, but this may be due to the fact that the reconnection apparently leads to high temperatures (i.e., the "spine," or large SXT loop) and the spatial resolution at these temperatures is just not adequate. *TRACE*-like resolution may be sufficient to observe such changes (Hudson 2000).

We cannot really ascribe a timescale to the topological changes. They may in fact occur smoothly, in the case of efficient reconnection in a highly resistive plasma. But this is somewhat counter to our intuition about the "catastrophic" nature of a flare. It is perfectly possible within this topological model to have the photospheric stressing cause current build-up in the coronal field without any (significant) reconnection, although the field itself would become increasingly nonpotential. (Note again that the potential extrapolation used in the topological model should nonetheless adequately represent the connectivities even in a nonpotential field.) At some single, critical level of stressing, or possibly in several "bursty" reconnection episodes, the reconnection occurs, taking the system to a final, potential configuration. The time, or the rate, or the manner of the reconnection are not specified, but the changes in

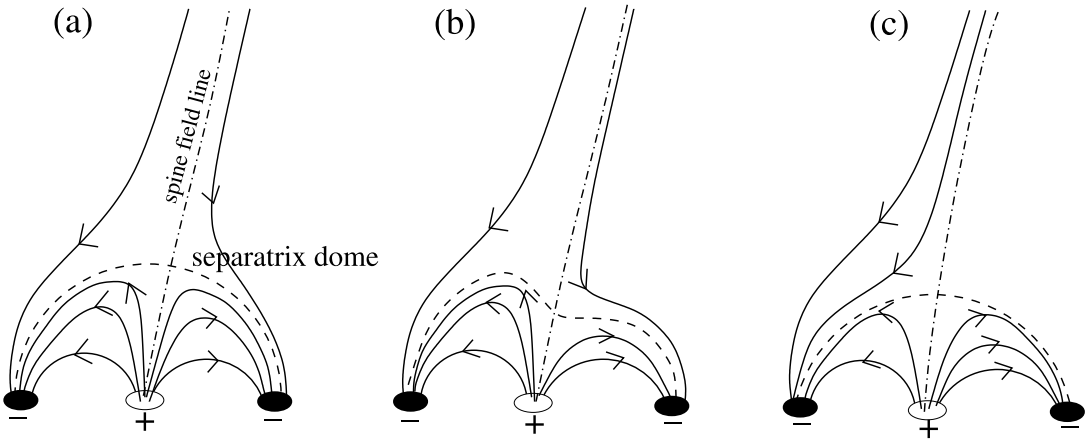

FIG. 11.—Two-dimensional representation of the process of reconnection via a separator dome

connectivity, which are our main concern here, depend only on the topology.

Although we must be cautious of the lack of physics in this model, it does provide an interesting comparison with many of the features which we see in the flare. Most importantly, it demonstrates that cancellation of small magnetic elements, possibly indicated in the observations by kernel brightenings near the interface of opposite polarities, can cause reconfiguration of the large-scale field. Based on the model and observations, we expect that the flare occurs as a result of coronal field stressed by small-scale photospheric flux motions and cancelation, at the interface between the PFC and strong negative field to the southwest.

A number of other observed phenomena can be explained by this model. It shows how flux cancellation causes field lines to open at a different location, as suggested by the observed *TRACE* ejecta which occur at a different location to the preflare brightenings. This happens because field lines are reconnecting into the segment in which the flux cancelation event took place, so the outward-reconnecting field lines cannot originate in that same segment. The bright SXT core/EUV loop in both the flare and preflare phases may indicate the position of heated separators, either because of Joule heating by currents as predicted in the MCC model of Longcope (1996) or by ongoing low-level fan reconnection. Heating of the large SXT loop before and during the flare is likewise consistent with heating or reconnection occurring at a spine fieldline. The cusplike shape of the ejecta is due to the shape of newly reconnected field lines around the separatrix dome and spine.

In this model, the preflare activity could be explained as flux cancellation occurring more slowly than in the large flare, so that the preflare is a less energetic version of the main flare. The site of preflare activity would therefore be a very good predictor of the site where a large flare would occur, should the photospheric driving suddenly increase, while the duration of the flare would be determined to a great extent by the size of the cancelling features and the speed with which they come together. By contrast, one would expect the total energy released in the flare to be determined by both the free energy in the coronal field and the footpoint driving.

The simultaneously brightening EUV kernels (Fig. 4) can also be explained by the model in one of two ways. The first is that the EUV kernels are caused by chromospheric precipitation of beams accelerated at the coronal null (see discussion in § 5), through which passes the diverging fan of field lines of the separatrix dome. Alternatively, each EUV kernel may indicate the position of a separatrix surface between the flux "segments" within the dome, where reconnection between neighboring flux systems is taking place. In either case, the EUV sources may be caused by bombardment of the chromosphere, following particle acceleration in a complex reconnecting magnetic geometry.

The model is of course a significant simplification of the true corona. It uses a vacuum potential field extrapolation, and gravitational forces and pressure gradients are assumed to be dominated by magnetic forces. Furthermore, the model is not genuinely time dependent. But despite its simplicity the model does predict where reconnection is likely to happen, and how the field adjusts in response to it. Thus it is a very instructive tool for studying a complex reorganization process. Future resistive MHD models will doubtless be able to build in more physics, for example using observations such as the "traveling blob" observed in Lyα (Fig. 8). This blob moves slowly around the structure, close to the apparent base of the ejecta, and we speculate that it is related to the location at which field lines open to eject material. In our model, this location also moves slowly through the structure compared to the speed at which field lines move through the coronal null, and the path it follows will depend on the speed of the footpoint flux cancellation and the field topology. The Lyα observations may thus assist in better understanding the field geometry and photospheric driving.

5. DISCUSSION AND CONCLUSIONS

We have presented a set of observations and a model which together suggest a topological explanation for a single solar flare event. We now discuss some further, more general implications of our work as well as pointing out its shortcomings and possible alternative interpretations for the event.

In § 3.3 we showed that the HXR and *TRACE* EUV flare kernels both have an impulsive appearance and peak within 90 s of one another. A temporal relationship between UV and X-ray impulsive-phase time profiles has been known since the 1970s, from *OSO-3* and *OSO-5* data (e.g., Kane & Donnelly 1971; Kane, Frost, & Donnelly 1979) and was also found by *SMM*, when HXRBS and UVSP light curves were seen to be simultaneous to within 1 s (Woodgate et al. 1983). It was speculated that the UV emission might be produced in the chromosphere by the same beam which generates the HXR emission, through heating (e.g., Poland et al. 1984; Emslie, Brown, & Donnelly 1978) or direct collisional excitation (e.g., Kane & Donnelly 1971). If it can be demonstrated that UV/EUV impulsive-phase emission is a proxy for electron beam deposition, this may provide further diagnostics in the study of nonthermal processes during flares. Since EUV and UV are far easier to image than HXR, an enhanced understanding of flare magnetic connectivity should follow. This will certainly be added to by the improved spatial and temporal resolution that will be attained by *HESSI*. Furthermore, by comparison with model calculations, we may also be able to use UV/EUV timing and intensity information as a beam diagnostic, much as is currently done with HXRs.

It has long been noted that the intensity of impulsive-phase HXR bursts suggest that a huge volume of plasma is necessary to provide the electrons to generate the observed emission. It is then a mystery how impulsive-phase signatures can be so rapid and coherent, as this implies that, within seconds, electrons from a volume of $(10{,}000\ \mathrm{km})^3$ pass through and are accelerated in a region which we expect to have a thickness of a few meters at most. This problem is avoided by postulating that the accelerator is constantly replenished by a return current. However, results by van Oss & van den Oord (1995) throw this into doubt. In an analytic beam electrodynamic calculation, these authors showed that the return current set up by a blunt, cylindrical, finite-duration beam as it propagates does not significantly penetrate the acceleration region on timescales shorter than a few magnetic diffusion times. The calculation may suggest that a return current is not a viable means of delivering fresh particles to the accelerator. We are left again with the implication that a large coronal volume is involved.

Our detailed data set provides the means to determine that this is also the case for the present flare, since with

forward modeling (see, e.g., Alexander & Metcalf 1997) we can predict the number of nonthermal electrons needed and compare this with density and volume estimates. Assuming that the HXR emission is nonthermal bremsstrahlung [the flare has very high counts in the M2 (33–53 keV) and HI (53–93 keV) channels of HXT and so is unlikely to be thermal], from a beam with form

$$F(E) = F_o E^{-\delta}, E > E_c ,$$

with cutoff energy E_c, we determine that the necessary integrated electron energy flux to give the observed maximum M1 and M2 counts is 4×10^{28} ergs s^{-1} for $E_c = 15$ keV and half this for $E_c = 30$ keV. This corresponds to an energy-integrated flux of $8(2) \times 10^{35}$ electrons cm^2 s^{-1} for a 15 (30) keV cutoff [since $N_{\rm tot} = (\delta - 1)F_{\rm tot}/(\delta - 2)E_c$ for this form of beam]. Approximating the HXR time profile by a symmetrical, triangular spike of approximately 50 s duration, we find that for a cutoff energy of 15 (30) keV, the total number of nonthermal electrons needed is $2(0.5) \times 10^{37}$.

Estimates from both *TRACE* and SXT give preflare densities in the brightest features of $\sim(0.7–2) \times 10^{10}$ cm^{-3}. Therefore, a minimum volume of $2.5(0.6) \times 10^{27}$ cm^3 (for $E_c = 15[30]$ keV) is needed to provide sufficient nonthermal electrons. The approximate volume contained within the separatrix dome (assuming this is a a hemispherical dome with a photospheric boundary marked by the EUV brightenings) is $\sim 3 \times 10^{27}$ cm^{-3}, so this could supply the electrons needed to produce HXRs in the chromosphere if all were accelerated. However, 100% efficient acceleration seems very unlikely. This suggests that, if we disallow the possibility of an accelerator replenished by a return current, electrons from outside the separatrix dome must enter and be accelerated. It is interesting that in our model the field is rapidly reconnecting and closing down near the location where HXR emission is observed. This process may provide a channel for electrons from the corona outside the separatrix dome to reach the reconnection region. Note that the process of inward reconnection of field lines through the separatrix dome may result in a situation akin to the "collapsing trap" accelerator of Somov & Kosugi (1997). In their model, first-order Fermi acceleration occurs in a shrinking magnetic geometry; it is conceivable that part of the reason for the HXR source being seen only at one location is that only at this location is a shrinking field geometry present.

We have observed a compact HXR footpoint, a large overlying loop which gradually brightens at high temperatures, particularly following the impulsive phase, and hot material traveling along the field at 100–200 km s^{-1}. Following the extensive theoretical and observational effort stimulated by *SMM*, this combination is now generally interpreted as chromospheric evaporation—the upward expansion of the rapidly heated chromosphere into a loop, following energy deposition by the beam which produced the HXRs, or by a heat flux. Our models and observations suggest a different scenario for this flare, one which recalls an interpretation of hot flare-related up-flows as being due to ejection of heated filament material (e.g., Bachelor & Hindsley 1991).

The up-flow we observe with *TRACE* takes place where field lines from within the separatrix dome are reconnecting to outside the dome. We propose therefore that the up-flowing material may be material which was on or supported by previously closed field lines and which is expelled outward as the field opens, driven by magnetic forces as the newly reconnected field straightens out. This provides the bulk motion aspect of "evaporation" in this flare. The brightening of the SXT loop at higher temperatures is a consequence of reconnection along the spine field line. Although we only have evidence for relatively cool (1 MK) ejecta and did not look for high-temperature moving material (which could be done with the *Yohkoh* Bragg Crystal Spectrometer) it is possible to see how strongly heated up- and down-flows could be produced in this model: the newly reconnected field lines have all passed through the reconnection site where, it is to be presumed, plasma heating takes place.

In other words, the observations normally counted as evidence for "evaporation" into a large overlying loop could, in this flare at least, be a combination of spine heating and material ejection, driven by the rearrangement of coronal field. There need be no involvement of the chromosphere, electron beams, or conduction at all. We have assumed that electron beams produce the HXR source, and must therefore generate a chromospheric response, but this may be limited to very small-scale closed field, rather than the large-scale flare loop. In such a compact configuration it is easy to see how the heated and up-flowing material, and the HXR footpoint, would occur in close proximity, and at low resolution appear consistent with the accepted view of evaporation.

However, the traditional evaporation scenario is supported by several observations, e.g., the observed momentum balance from red- and blueshifted lines (e.g., Zarro & Canfield 1989; Canfield et al. 1990), and the case for beam-driven evaporation is fairly robust. Furthermore, we cannot distinguish what is going on in the core of the flare, in the small bright SXT loops, which may well be filled by beam-driven evaporation. At the moment, we merely suggest this alternative, realizing that much further work would be necessary to demonstrate it. But models such as this may provide new stimulus for the discussion of observed phenomena such as pre- and postflare "evaporation" (e.g., Antonucci et al. 1985; Zarro & Lemen 1988) which would, in this model, be present for as long as photospheric driving led to coronal reconnection. Also, the "stationary component" (i.e., material which is heated but exhibits velocities several times lower than predicted by beam-driven evaporation models) which appears during even the earliest phases of the flare impulsive cannot be easily incorporated into the standard evaporation model (McClements & Alexander 1989). In our model this could be explained by heating due to rapid spine or fan reconnection, involving little mass motion.

The mention of ejected filament material leads us to discuss the possible role of a filament in this flare. As reported in §§ 3.2 and 3.4, *TRACE* observations in 171 Å suggest that there may be a filament overlying the neutral line between PFC and surrounding field, and the presence of ejecta suggests that it at least partially disappears during the event. In our model the filament material does not leave the active region; rather, the field lines supporting the filament material reconnect through the coronal null, so that the filament material can move from the field within the separatrix dome, and travel upward along the larger scale field. But there is no eruption as such. It would require a further reconnection with the global coronal field to allow the filament material to leave the Sun entirely. This is a

different viewpoint from that of the "standard" eruptive flare model in which reconnection behind an erupting filament allows it to travel outwards as a coronal mass ejection.

The energetic role of filaments in flares is also not clear; we take the view in this work that the energy for both flare and (if it occurs) filament ejection is the magnetic free energy of the corona without the filament, and that the filament passively does what the field dictates. However, there are models (e.g., Antiochos et al. 1999) in which the energy source powering the flare is the magnetic energy contained in the sheared or wound field associated with a filament at the core of the flare. In such models the flare topological evolution would be determined to a great extent by the relaxation of this filament field, rather than of the surrounding coronal field (which we model). However, as was pointed out by Antiochos et al. (1999), to access the energy of the core-field (alternatively, to permit the system of stressed core-field plus overlying field to reach lower energy states) in such "magnetic breakout" models, one must weaken the core-field confinement by allowing restructuring of the overlying corona. Should this occur because of footpoint driving, our model would still be useful in predicting how and where the initial opening of the overlying field would occur.

There are many physical quantities left unexplained by our topological model, such as the flare timescales, the energy budget, the rate at which the reconnection site moves through the flare, the velocity of ejected material, the location of particle acceleration, and the reason that high-energy particles are only clearly observed for a short time during the driving process. However, it provides a sufficiently interesting match with the observations to be worthy of further investigation. It remains to be seen whether this flare is one of a kind, or whether the separatrix dome configuration is a common one for compact flares. At the very least, the work presented here indicates how observations at high resolution and time cadence will improve our understanding of the evolution of the magnetic field and the location of particle acceleration in flares. On the basis of this study and others like it, we can expect significant advances from the combination of *TRACE*, SXT, and *HESSI* in the near future.

The task of analyzing data sets from multiple instruments is made immeasurably easier by the existence of the Solar-SoftWare system (Freeland & Handy 1998) and we thank all who contribute to this. L. F. thanks D. McKenzie for assistance with SXT data preparation, and M. Aschwanden, H. Hudson, N. Nitta, and K. Schrijver for useful discussion. We further thank an anonymous referee whose insightful comments have helped us improve both the manuscript and our understanding of the topological model. L. A. R. acknowledges the support of a Lockheed Martin Summer Internship. D. S. B. thanks the UK Particle Physics and Astronomy Research Council for financial support and Lockheed Martin Solar and Astrophysics Lab (LMSAL) travel support. This work was carried out under NASA contracts NS8-37334 (SXT) and NAS5-38099 (*TRACE*). The *Yohkoh* SXT project is a collaborative project of LMSAL, the National Astronomical Observatory of Japan, and the University of Tokyo, supported by NASA and ISAS. *TRACE* is operated jointly out of Goddard Space-flight Center by scientists from the University of Chicago, Montana State University, LMSAL, and the Harvard-Smithsonian Center for Astrophysics.

REFERENCES

Alexander, D. 1999, J. Geophys. Res., 104, 9701
Alexander, D., & Metcalf, T. R. 1997, ApJ, 489, 442
Antiochos, S. 1998, ApJ, 502, L181
Antonucci, E., Dennis, B. R., Gabriel, A. H., & Simnett, G. M. 1985, Sol. Phys., 96, 129
Aschwanden, M. J., Hudson, H., Kosugi, T., & Schwartz, R. A. 1996a, ApJ, 464, 985
Aschwanden, M. J., Wills, M. J., Hudson, H. S., Kosugi, T., & Schwartz, R. A. 1996b, ApJ, 468, 398
Aulanier, G., DeLuca, E. E., Antiochos, S. K., McMullen, R. A. & Golub, L. 2000, ApJ, 540, 1126
Bachelor, D. A., & Hindsley, K. P. 1991, Sol. Phys., 135, 99
Brown, D. S., & Priest, E. R. 1999, Proc. R. Soc. London A, 455, 3931
———. 2000, Sol. Phys., 194, 197
Canfield, R. C., Metcalf, T. R., Zarro, D. M., & Lemen, J. R. 1990, ApJ, 348, 333
Canfield, R. C., Zarro, D. M., Wülser, J.-P., & Dennis, B. R. 1991, ApJ, 367, 671
Craig, I. J. D., & McClymont, A. N. 1999, ApJ, 510, 1045
Demoulin, P., van Driel-Gesztelyi, L., Schmieder, B., Hénoux, J. C., Csepura, C., & Hagyard, M. J. 1993, A&A, 271, 292
Donnelly, R. F., & Kane, S. R. 1978, ApJ 222, 1043
Emslie, A. G., Brown, J. C., & Donnelly, R. F. 1978, Sol. Phys., 57, 175
Freeland, S. L. & Handy, B. N. 1998, Sol. Phys., 182, 497
Handy, B. N., et al. 1999, Sol. Phys., 187, 229
Hanoaka, Y. 1997, Sol. Phys., 173, 319
Hudson, H. S. 2000, ApJ, 531, L75
Hudson, H. S., & Wheatland, M. S. 1999, Sol. Phys., 186, 301
Kane, S. R., & Donnelly R. F. 1971, ApJ, 164, 151
Kane, S. R., Frost, K. J., & Donnelly, 1979, ApJ, 234, 669
Kosugi, T., et al. 1991, Sol. Phys., 136, 17
Lau, Y. -T., & Finn, J. M. 1990, ApJ, 350, 672
Longcope, D. W. 1996, Sol. Phys. 169, 91
Longcope, D. W., & Silva, A. V. R. 1998, Sol. Phys., 179, 349
McClemets, K. G., & Alexander, D. 1989, Sol. Phys., 123, 161
McKenzie, D. E., & Hudson, H. S. 1999, ApJ, 519, L93
Metcalf, T. R., Hudson, H. S., Kosugi, T. Pueter, R. C., & Pinã, R. K. 1996, ApJ, 466, 585
Nishio, M., Yaji, K., Kosugi, T., Nakajima, H., & Sakurai, T. 1997, ApJ, 489, 976
Poland, A. I., Orwig, L. E., Mariska, J. T., Auer, L. H., & Nakatsuka, R. 1984, ApJ, 280, 457
Priest, E. R., Bungey, T. N., & Titov, V. S. 1997, Geophys. Astrophys. Fluid Dyn., 84, 127
Priest, E. R., & Titov, V. S. 1996, Phil. Trans. R. Soc., 354, 2951
Schrijver, C. J., et al. 1999, Sol. Phys., 187, 261
Shibata, K., Ishido, Y., Acton, L. W., Strong, K. T., & Hirayama, T. 1992, PASJ, 44, L173
Somov, B. V., & Kosugi, T. 1997, ApJ, 485, 859
Sweet, P. A. 1969, ARA&A, 7, 149
Tsuneta, S. 1996, ApJ, 456, 840
Tsuneta, S., et al. 1991, Sol. Phys, 136, 37
———. 1992, PASJ, 44, L63
van Oss, R. F., & van den Oord, G. H. J. 1995, A&A, 299, 297
Woodgate, B. E., Shine, R. A., Poland, A. I., & Orwig, L. E. 1983, ApJ, 265, 530
Zarro, D. M., & Canfield, R. C. 1989, ApJ, 338, L33
Zarro, D. M., & Lemen, J. R. 1988, ApJ, 329, 456